INTERNATIONAL JOURNAL OF PHARMACEUTICAL SCIENCES
[ISSN: 0975-4725; CODEN(USA): IJPS00]
Journal Homepage: https://www.ijpsjournal.com

OPEN ACCESS

Research Article

Development and Characterization of Oroxylin a Loaded Functionalized Inhalable Microspheres for Targeted Delivery in Lung Cancer

Mayur Avinash Lawande*, Wagh.j.G

Department of Pharmaceutical Quality Assurance, MES'S College of Pharmacy, Sonai, Ahmednagar, Maharashtra, India

ARTICLE INFO

Published: 27 May. 2026
Keywords:
Oroxylin A, Inhalable microspheres, Ionotropic gelation, Pulmonary drug delivery, Boswellia serrata gum.
DOI:
10.5281/zenodo.20416115

ABSTRACT

The present study focused on the development, optimization, and evaluation of inhalable oroxylin A-loaded microspheres using sodium alginate and Boswellia serrata gum prepared by ionotropic gelation for pulmonary drug delivery. Oroxylin A, a poorly water-soluble BCS Class II flavonoid (0.08 ± 0.01 mg/mL), was characterized by UV, DSC, FTIR, and melting point analysis, confirming its identity and purity. Drug–excipient compatibility studies showed no significant interactions.A 3^2 full factorial design was used to optimize nine formulations (F1–F9). The microspheres exhibited particle sizes of 1.82–4.86 µm, zeta potential of −18.42 to −32.58 mV, entrapment efficiency of 62.18–85.42%, and sustained drug release up to 12 hours. The optimized formulation F1 showed the smallest respirable particle size (1.82 ± 0.14 µm) and highest drug release (92.14 ± 2.48%), following Higuchi diffusion kinetics (R^2 = 0.9946). ANOVA confirmed the significance of the quadratic model. Stability studies conducted as per ICH guidelines demonstrated satisfactory stability for three months at room temperature. The developed inhalable microspheres show promise as an effective pulmonary drug delivery system for oroxylin A.

INTRODUCTION

1.1 Lung Cancer

Lung cancer remains one of the most significant challenges in modern oncology, characterized by the uncontrolled proliferation of abnormal lung cells with the potential for invasion and metastasis. Despite advances in diagnosis and treatment, it continues to be the leading cause of cancer-related mortality worldwide, exceeding the combined deaths from breast, prostate, and colorectal cancers [1]. The heterogeneous nature of lung tumors, combined with the tendency for late stage

***Corresponding Author:** Mayur Avinash Lawande
Address: *Department of Pharmaceutical Quality Assurance, MES'S College Of Pharmacy, Sonai, Ahmednagar, Maharashtra, India.*
Email ✉: mayurlawande5385@gmail.com
Relevant conflicts of interest/financial disclosures: The authors declare that the research was conducted in the absence of any commercial or financial relationships that could be construed as a potential conflict of interest.

diagnosis, creates a clinical scenario where treatment outcomes remain suboptimal for the majority of patients. Understanding the fundamental aspects of this disease, including its epidemiology, pathological classification, molecular underpinnings, and existing therapeutic landscape, is essential for identifying opportunities to develop more effective and targeted treatment strategies [2].

1.2 Global Epidemiology and Disease Burden of Lung Cancer

Lung cancer stands as the second most commonly diagnosed malignancy and the primary cause of cancer related deaths on a global scale. According to GLOBOCAN estimates published by the International Agency for Research on Cancer, approximately 2.48 million new cases of lung cancer were reported in 2022, accounting for nearly 12.4% of all new cancer diagnoses worldwide. In the same year, lung cancer was responsible for approximately 1.82 million deaths, representing roughly 18.7% of all cancer related fatalities. These figures underscore the enormous burden that this disease places on healthcare systems across both developed and developing nations. The incidence rates exhibit significant geographic variation, with the highest rates observed in East Asia, Europe, and North America, largely attributable to differences in tobacco consumption patterns and environmental exposures [5].

The epidemiological profile of lung cancer has undergone notable shifts over recent decades. While incidence rates among males have shown a declining trend in many high income countries, largely as a consequence of successful tobacco control measures and public health campaigns, rates among females have either plateaued or continued to increase in several regions. This gender based divergence reflects historical differences in smoking adoption and cessation patterns. Furthermore, an increasing proportion of lung cancer cases are being diagnosed in individuals who have never smoked, suggesting that non tobacco risk factors such as air pollution, occupational exposures, radon gas, and genetic predisposition are playing an increasingly important role in disease etiology. The rising incidence in never smokers has prompted a reevaluation of screening strategies and risk assessment models [6].

1.3 Classification of Lung Cancer and Pathological Subtypes

Lung cancer is broadly classified into two principal histological categories based on morphological characteristics, biological behavior, and clinical management strategies: non small cell lung cancer (NSCLC) and small cell lung cancer (SCLC). This classification system holds fundamental importance in clinical oncology as it directly governs the choice of treatment modality, predicts prognosis, and informs decisions regarding surgical candidacy. Non small cell lung cancer accounts for approximately 80 to 85% of all lung cancer diagnoses and encompasses several distinct subtypes, each with unique histopathological features, molecular profiles, and clinical behaviors. Small cell lung cancer, representing the remaining 15 to 20% of cases, is characterized by rapid proliferation, early and widespread metastatic dissemination, and an initial but often short lived responsiveness to chemotherapy and radiation [9].

Non small cell lung cancer is further subdivided into three major histological subtypes: adenocarcinoma, squamous cell carcinoma, and large cell carcinoma. Adenocarcinoma is currently the most prevalent subtype, accounting for approximately 40 to 50% of all NSCLC cases. It typically arises from the mucus secreting glandular

cells lining the peripheral airways and alveoli, and is the most common subtype observed in never smokers, women, and younger patients. Histologically, adenocarcinoma may display diverse growth patterns including lepidic, acinar, papillary, micropapillary, and solid patterns, which carry important prognostic implications. The World Health Organization classification system, most recently updated in 2021, provides a detailed framework for subclassifying adenocarcinomas based on predominant architectural patterns, with micropapillary and solid predominant subtypes associated with more aggressive clinical behavior and poorer survival outcomes [10].

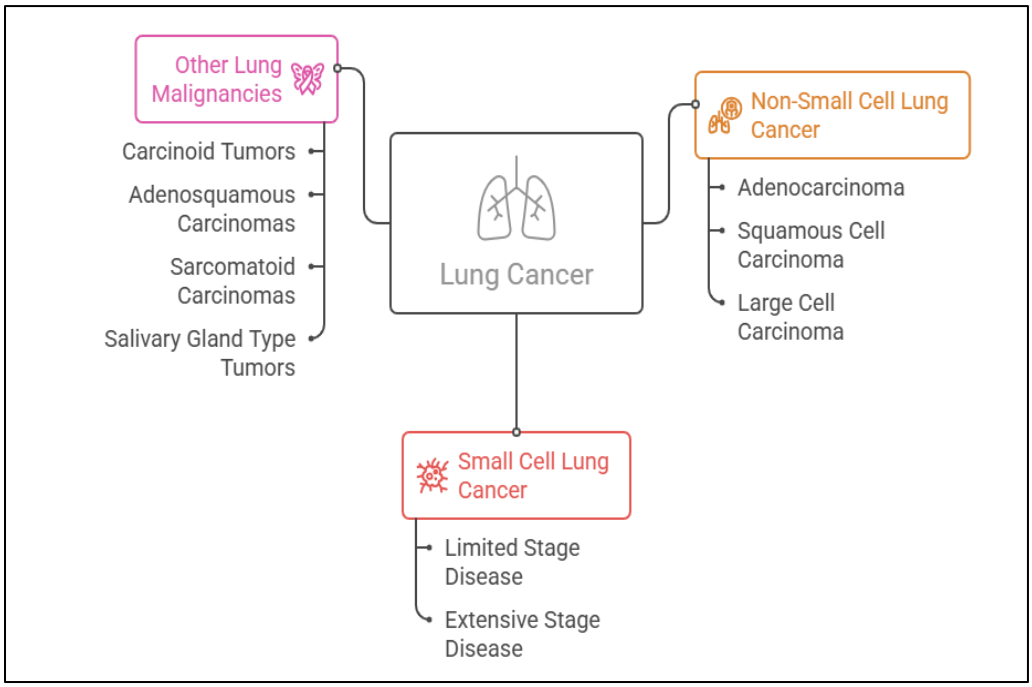

Figure 1: Histological Classification of Lung Cancer Subtypes

1.4 Current Diagnostic Approaches for Lung Cancer

Early and accurate diagnosis of lung cancer is a critical determinant of treatment success and patient survival, yet the disease continues to present significant diagnostic challenges owing to its frequently insidious onset and nonspecific symptomatology. The diagnostic workup for suspected lung cancer typically involves a multimodal approach integrating clinical evaluation, radiological imaging, tissue sampling, and molecular profiling. The following are the major diagnostic modalities currently employed in clinical practice for the detection, characterization, and staging of lung cancer [23].

1.2.0 Materials And Methods:

1.2.1 Materials:

The materials used in the study were procured from various standard commercial sources. Oroxylin A was obtained from Sciquaint Innovations Pvt. Ltd. (Pune, India). Polymers and natural gums, including Sodium Alginate and Potassium Bromide (KBr), were sourced from Loba Chemie Pvt. Ltd. (Mumbai, India), while Boswellia serrata Gum was procured from Herbo Nutra (New Delhi, India).

Chemical reagents such as Calcium Chloride, Hydrochloric Acid (0.1 N), Acetone, and Ethyl Acetate were supplied by SD Fine-Chem Ltd. (Mumbai, India). Methanol and Dimethyl Sulfoxide (DMSO) were obtained from Merck Life Science Pvt. Ltd. (Mumbai, India).

Phosphate Buffer Saline (PBS) pH 7.4 was sourced from HiMedia Laboratories Pvt. Ltd. (Mumbai, India), and Chloroform was procured from Loba Chemie Pvt. Ltd. (Mumbai, India). Additionally, Ethanol was acquired from Changshu Hongsheng Fine Chemical Co. Ltd. (India), and Distilled Water was prepared in-house for all experimental requirements.

1.2.2. Organoleptic Evaluations of Oroxylin A

The organoleptic properties of oroxylin A were evaluated visually and physically to confirm the identity and purity of the procured drug sample. The color of the pure drug was assessed by placing the sample on a clean white porcelain tile and observing under natural daylight conditions. The odor was determined by wafting a small quantity of the sample towards the nose, following standard sensory evaluation practices. The texture was assessed by gently rubbing a small amount of the drug between the thumb and index finger to determine its physical feel. All organoleptic evaluations including color, odor, and texture were performed independently by three trained observers (n=3) and the observations were recorded. The results were compared with the reported organoleptic characteristics available in the published literature to confirm the identity of the received sample [24].

1.2.3. Scanning Absorbance Maxima Determination of Oroxylin A

The absorbance maxima (λ_{max}) of oroxylin A was determined using a UV-Visible spectrophotometer (Shimadzu UV-1800, Shimadzu Corporation, Kyoto, Japan). A stock solution was prepared by accurately weighing 10 mg of oroxylin A and transferring it into a 100 ml volumetric flask, dissolved in methanol, and the volume was made up to the mark with methanol to obtain a concentration of 100 µg/ml. The stock solution was sonicated using a bath sonicator (Remi Elektrotechnik Ltd., Mumbai, India) to ensure complete dissolution of the drug. From this stock solution, 1 ml was pipetted out and transferred into a 10 ml volumetric flask and the volume was made up to the mark with methanol to obtain a working concentration of 10 µg/ml. The prepared solution was transferred into a quartz cuvette of 1 cm path length and scanned over the wavelength range of 200–400 nm against methanol as a blank. The scanning was performed at medium scan speed with a spectral bandwidth of 1.0 nm and a sampling interval of 0.5 nm. The wavelength corresponding to the maximum absorbance was recorded as the λ_{max} of oroxylin A. The determination was performed in triplicate (n=3) and the mean λ_{max} value was reported. The obtained λ_{max} was compared with the values reported in the published literature to confirm the identity of the drug [25].

1.2.4. Calibration Curve Determination

The calibration curve of oroxylin A was established in methanol using a UV-Visible spectrophotometer (Shimadzu UV-1800, Shimadzu Corporation, Kyoto, Japan) at the predetermined λ_{max}. A stock solution was prepared by accurately weighing 10 mg of oroxylin A and transferring it into a 100 ml volumetric flask, dissolved in methanol, and the volume was made up to the mark with methanol to obtain a concentration of 100 µg/ml. The stock solution was sonicated using a bath sonicator (Remi Elektrotechnik Ltd., Mumbai, India) to ensure

complete dissolution of the drug. From this stock solution, appropriate aliquots of 0.2, 0.4, 0.6, 0.8, 1.0, and 1.2 ml were pipetted out and transferred into separate 10 ml volumetric flasks, and the volume of each was made up to the mark with methanol to obtain working concentrations of 2, 4, 6, 8, 10, and 12 µg/ml, respectively. The absorbance of each solution was measured at the determined λ_{max} using a quartz cuvette of 1 cm path length against methanol as a blank. The measurements were performed in triplicate (n=3) and the mean absorbance values were recorded. The calibration curve was constructed by plotting the mean absorbance values on the Y-axis against the corresponding concentrations (µg/ml) on the X-axis. The linearity of the calibration curve was assessed by linear regression analysis, and the equation of the line ($y = mx + c$) along with the coefficient of determination (R^2) was calculated using Microsoft Excel (Microsoft Corporation, Redmond, USA). The calibration curve was considered linear if the R^2 value was found to be ≥ 0.999 [26].

1.2.5. Experimental design

A 3^2 full factorial design was employed to optimize the formulation of oroxylin A loaded inhalable microspheres using Design-Expert software (Stat-Ease Inc., Minneapolis, USA). Two independent variables were selected at three levels: boswellia serrata gum concentration (X_1) at 0.65, 0.70, and 0.75 % w/v as low (-1), medium (0), and high (+1) levels, respectively, and sodium alginate concentration (X_2) at 0.50, 1.50, and 2.50 % w/v as low (-1), medium (0), and high (+1) levels, respectively. The design generated a total of 9 experimental runs with all possible combinations of the two factors at three levels. The dependent variables selected for evaluation were particle size (Y_1) and in vitro drug release at 12 hours (Y_2). The relationship between the independent and dependent variables was established using the following general polynomial equation:

$$Y = \beta_0 + \beta_1 X_1 + \beta_2 X_2 + \beta_{12} X_1 X_2 + \beta_{11} X_1^2 + \beta_{22} X_2^2$$

where Y is the measured response, β_0 is the intercept, β_1 and β_2 are the linear coefficients, β_{12} is the interaction coefficient, and β_{11} and β_{22} are the quadratic coefficients of the independent variables X_1 and X_2, respectively. The statistical significance of the model was evaluated by analysis of variance (ANOVA) at a significance level of $p < 0.05$. The optimized formulation was selected based on the desirability function approach and the experimental values were compared with the predicted values to validate the design [27,28].

Table1.1: Variables in 3^2 factorial design for Oroxylin A loaded inhalable microsphere formulations

Independent Variables	Levels		
	Low	Medium	High
X_1: *Boswellia serrata* gum (%)	0.55	0.65	0.75
X_2: Sodium Alginate (%)	0.50	1.50	2.50
Dependent Variables			**Goal**
Y_1: Particle Size (µm)			Minimize
Y_4: In vitro Drug Release (%)			Maximize

1.2.6. Formulation of Oroxylin A Loaded Inhalable Microspheres

Oroxylin A loaded inhalable microspheres were prepared by the ionotropic gelation method. Sodium alginate and *Boswellia serrata* gum were accurately weighed as per the 3^2 factorial design and dissolved in distilled water under continuous stirring using a magnetic stirrer (Remi Elektrotechnik Ltd., Mumbai, India) at 500 rpm for 30 minutes to obtain a homogeneous polymer solution. An accurately weighed quantity of oroxylin A (equivalent to the target drug loading) was dispersed in the polymer solution and stirred continuously for an additional 15 minutes to ensure uniform distribution of the drug within the polymer matrix. The resulting drug-polymer dispersion was then extruded dropwise through a 22-gauge hypodermic needle into a calcium chloride cross-linking solution (5 % w/v) maintained under gentle agitation at 100 rpm using a magnetic stirrer. Upon contact with the calcium chloride solution, the droplets instantaneously gelled to form discrete microspheres due to the ionic cross-linking between the calcium ions and the carboxylate groups of sodium alginate. The formed microspheres were allowed to remain in the cross-linking solution for 30 minutes to ensure complete curing and adequate mechanical strength. The microspheres were then collected by filtration, washed three times with distilled water to remove excess calcium chloride and any unentrapped drug, and subsequently dried at room temperature for 24 hours. A total of 9 formulation batches (F1–F9) were prepared as per the experimental design and the dried microspheres were stored in airtight containers in a desiccator until further evaluation. All formulations were prepared in triplicate (n=3) [29,30].

Table 1.2: Composition of Oroxylin a Loaded Inhalable Microspheres (F1–F9)

Formulation Code	Oroxylin A (mg)	*Boswellia serrata* Gum (% w/v)	Sodium Alginate (% w/v)	Calcium Chloride (% w/v)	Distilled Water (ml)
F1	50	0.65	0.50	5.0	50
F2	50	0.65	1.50	5.0	50
F3	50	0.65	2.50	5.0	50
F4	50	0.70	0.50	5.0	50
F5	50	0.70	1.50	5.0	50
F6	50	0.70	2.50	5.0	50
F7	50	0.75	0.50	5.0	50
F8	50	0.75	1.50	5.0	50
F9	50	0.75	2.50	5.0	50

2.1: Evaluation of Formulation:

2.1.1 Organoleptic Evaluations of Oroxylin A

The organoleptic evaluation of oroxylin A revealed that the procured drug sample exhibited a yellowish color, characteristic odor, and fine powder texture, which were found to be consistent with the standard reported values in the published literature. The concordance between the observed and standard organoleptic parameters confirmed the identity and authenticity of the received oroxylin A sample. The absence of any deviation in color, odor, or texture indicated that the drug was free from any visible contamination or

degradation, thereby confirming its suitability for further formulation development studies.

Table 2.1: Organoleptic Evaluation of Oroxylin A

Sr. No.	Parameters	Observed	Standard
1	Color	Yellowish	Yellowish
2	Odor	Characteristic odor	Characteristic odor
3	Texture	Fine powder	Fine powder

2.1.2. Particle Size Analysis

The particle size of oroxylin A loaded inhalable microspheres was determined using an optical microscope (Labomed Lx400, Labomed Inc., Mumbai, India) fitted with a calibrated stage micrometer and eyepiece micrometer. A small quantity of microspheres from each formulation batch was spread on a clean glass slide and observed under the microscope at a suitable magnification. The diameters of randomly selected 100 microspheres from each batch were measured using the calibrated eyepiece micrometer. The mean particle size and standard deviation were calculated for each formulation. The measurement was performed in triplicate (n=3) and the average particle size was expressed in micrometers (µm) [31].

2.1.3 Percentage Yield

The percentage yield of oroxylin A loaded inhalable microspheres was determined for each formulation batch. The prepared microspheres were collected after drying and weighed accurately using a digital analytical balance (Shimadzu AUX220, Shimadzu Corporation, Kyoto, Japan). The percentage yield was calculated by comparing the practical weight of the obtained microspheres with the total theoretical weight of all the solid components including oroxylin A, sodium alginate, and *Boswellia serrata* gum used in the formulation. The determination was performed in triplicate (n=3) and the mean percentage yield along with standard deviation was reported for each batch [32].

2.1.4 Characterization of Oroxylin A loaded Inhalable Microspheres

The particle size of oroxylin A loaded inhalable microspheres ranged from 1.82 ± 0.14 µm (F1) to 4.86 ± 0.17 µm (F9), indicating that all formulations fell within the respirable size range suitable for pulmonary drug delivery. An increase in the concentrations of both sodium alginate and *Boswellia serrata* gum resulted in a progressive increase in particle size, attributable to the higher viscosity of the polymer solution leading to larger droplet formation during ionotropic gelation. The zeta potential values ranged from -18.42 ± 1.12 mV (F1) to -32.58 ± 1.74 mV (F9), with all formulations exhibiting negative surface charges, indicating good physical stability of the microspheres due to electrostatic repulsion preventing aggregation. The percentage yield ranged from 72.34 ± 1.46% (F1) to 88.64 ± 1.38% (F9), demonstrating that higher polymer concentrations contributed to improved yield due to enhanced cross-linking efficiency with calcium chloride ions.

Table 2.2: Particle Size, Zeta Potential and Percentage Yield of Oroxylin A Loaded Inhalable Microspheres

Formulation Code	Particle Size (µm)	Zeta Potential (mV)	Percentage Yield (%)
F1	1.82 ± 0.14	-18.42 ± 1.12	72.34 ± 1.46
F2	2.94 ± 0.18	-22.56 ± 1.34	76.82 ± 1.28
F3	3.58 ± 0.21	-25.38 ± 1.56	79.56 ± 1.52
F4	2.46 ± 0.16	-20.74 ± 1.28	75.18 ± 1.34
F5	3.72 ± 0.22	-26.82 ± 1.42	82.46 ± 1.18
F6	4.18 ± 0.19	-29.14 ± 1.68	85.72 ± 1.56
F7	2.78 ± 0.15	-21.86 ± 1.18	78.24 ± 1.42
F8	4.25 ± 0.24	-28.46 ± 1.52	84.38 ± 1.64
F9	4.86 ± 0.17	-32.58 ± 1.74	88.64 ± 1.38

All values are expressed as mean ± SD (n=3)

The drug entrapment efficiency of oroxylin A loaded inhalable microspheres ranged from 62.18 ± 1.54% (F1) to 85.42 ± 1.66% (F9), while the drug loading capacity ranged from 8.24 ± 0.42% (F1) to 16.82 ± 0.52% (F9). A progressive increase in both parameters was observed with increasing concentrations of sodium alginate and *Boswellia serrata* gum across the formulations. This enhancement can be attributed to the formation of a denser and more compact polymer matrix at higher polymer concentrations, which provided greater drug retention capacity and minimized drug loss during the cross-linking process with calcium chloride. Formulation F9, with the highest polymer concentrations, demonstrated the maximum entrapment efficiency and drug loading, suggesting that an optimized polymer ratio is essential for achieving efficient drug encapsulation within the microspheres.

3.0 Results and Discussion:

3.1.1 Organoleptic Evaluations of Oroxylin A

The organoleptic evaluation of oroxylin A revealed that the procured drug sample exhibited a yellowish color, characteristic odor, and fine powder texture, which were found to be consistent with the standard reported values in the published literature. The concordance between the observed and standard organoleptic parameters confirmed the identity and authenticity of the received oroxylin A sample. The absence of any deviation in color, odor, or texture indicated that the drug was free from any visible contamination or degradation, thereby confirming its suitability for further formulation development studies.

Table 3.1: Organoleptic Evaluation of Oroxylin A

Sr. No.	Parameters	Observed	Standard
1	Color	Yellowish	Yellowish
2	Odor	Characteristic odor	Characteristic odor
3	Texture	Fine powder	Fine powder

3.1.2. Calibration Curve Determination

The calibration curve of oroxylin A in methanol was established at 273 nm over the concentration range of 2–12 µg/ml. The absorbance values increased linearly with increasing concentration, demonstrating excellent linearity with a correlation coefficient (R^2) of 0.9997, which exceeded the acceptable limit of 0.999. The equation of the regression line was obtained as y = 0.0563x + 0.0025, with a slope of 0.0563 and an intercept of 0.0025, indicating negligible deviation from the origin. The high degree of linearity confirmed that the developed method obeyed Beer-Lambert's law within the selected concentration range and was suitable for accurate quantitative estimation of oroxylin A in subsequent formulation studies.

Table 3.2: Calibration Curve Data of Oroxylin A in Methanol

Sr. No.	Concentration (µg/ml)	Absorbance
1	0	0.000
2	2	0.112
3	4	0.237
4	6	0.339
5	8	0.453
6	10	0.564
7	12	0.678
Slope		0.0563
Intercept		0.0025
Correlation Coefficient		0.9997
Absorbance Maxima		273

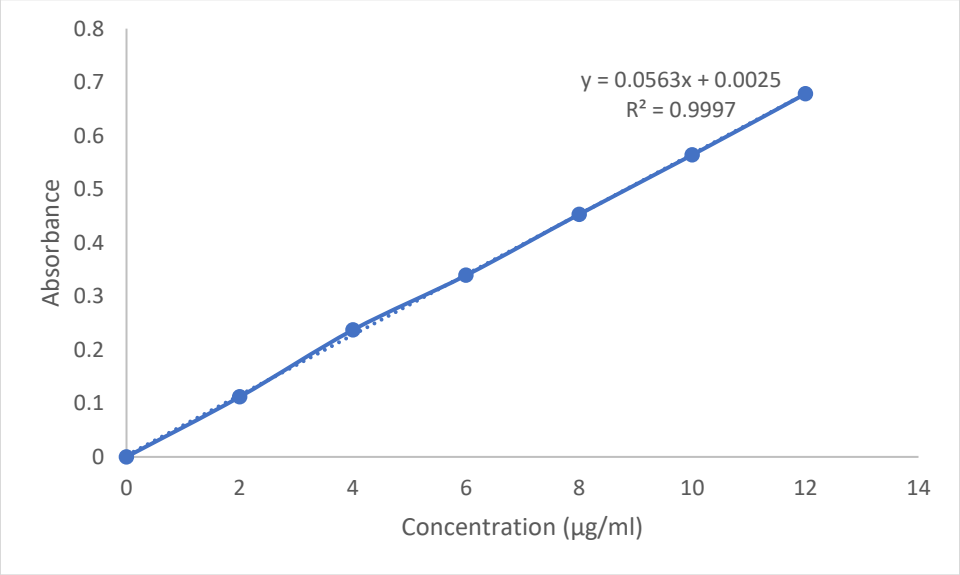

Figure 3.3: Calibration Curve of Oroxylin A in methanol

3.1.3. Melting point determination

The melting point of oroxylin A was determined in triplicate and found to be 232.33 ± 0.58°C, which

was in close agreement with the reported literature value of 231–233°C. The narrow melting range and minimal standard deviation indicated the high purity and crystalline nature of the procured drug sample. The absence of any significant deviation from the reported melting point confirmed that the drug was free from impurities or polymorphic modifications, thereby establishing its identity and suitability for use in the formulation of inhalable microspheres.

Table 3.4: Melting Point Determination of Oroxylin A

Sr. No.	Compound	Melting Point Observed (°C)	Melting Point Reported (°C)
1	Oroxylin A	232.33 ± 0.58	231–233

3.1.4. DSC Analysis

The DSC thermogram of pure oroxylin A exhibited a sharp endothermic peak at 232.65°C, corresponding to its melting point, which confirmed the crystalline nature and purity of the drug. The DSC thermogram of the physical mixture of oroxylin A with sodium alginate and *Boswellia serrata* gum displayed an additional broad endothermic peak at 78.90°C, attributable to the dehydration of the polymeric excipients, along with the characteristic drug peak at 232.48°C. The retention of the drug's endothermic peak in the physical mixture with only a negligible shift of 0.17°C confirmed the absence of any significant physical incompatibility between oroxylin A and the selected excipients, indicating their suitability for microsphere formulation.

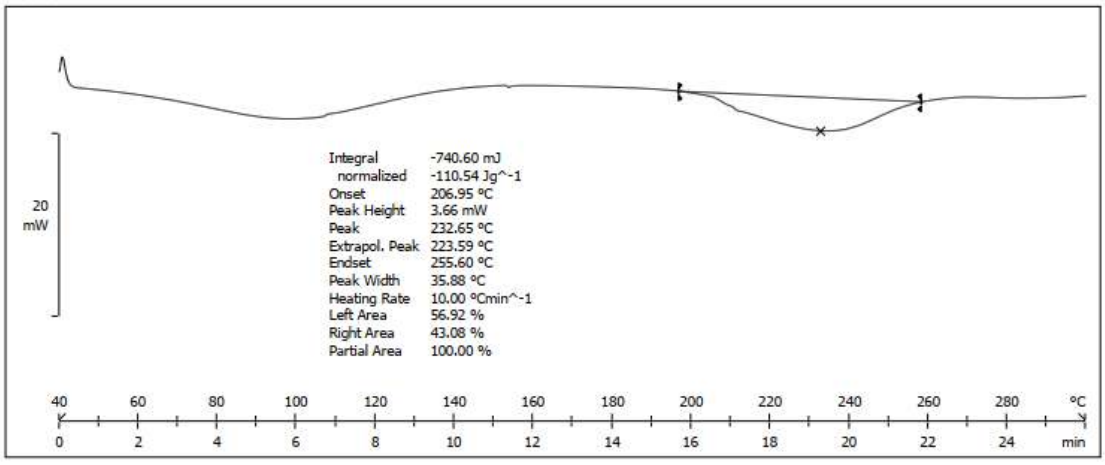

Figure 3.4: DSC Spectra of Pure Oroxylin A (232.65°C)

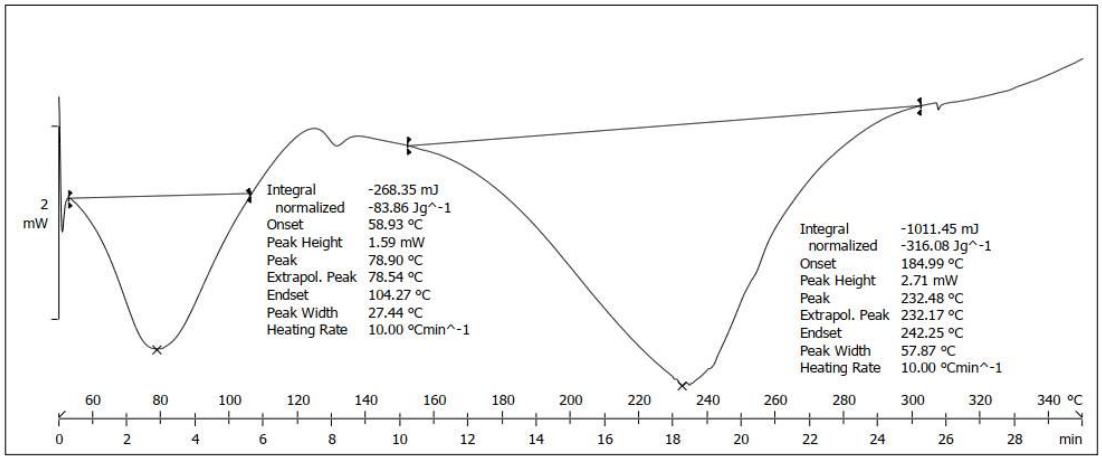

Figure 3.5: DSC Spectra of Physical Mixture (78.90 and 232.48)

3.1.5 FTIR Analysis

The FTIR spectrum of pure oroxylin A displayed all characteristic absorption bands including O–H stretching (3336.59 cm^{-1}), C–H aromatic stretching (3082.31, 3050.83 cm^{-1}), C=O carbonyl stretching (1651.13 cm^{-1}), C=C aromatic stretching (1611.30, 1571.20 cm^{-1}), and C–O–C ether stretching (1259.70, 1206.59 cm^{-1}), confirming the structural identity of the drug. The FTIR spectra of sodium alginate and *Boswellia serrata* gum exhibited their respective characteristic peaks within the standard wavenumber ranges. The physical mixture spectrum retained all principal absorption bands of oroxylin A with only minor shifts in wavenumber values, and no disappearance of existing peaks or emergence of new peaks was observed. These findings confirmed the absence of any chemical interaction or incompatibility between oroxylin A and the selected polymeric excipients, thereby supporting their combined use in the microsphere formulation.

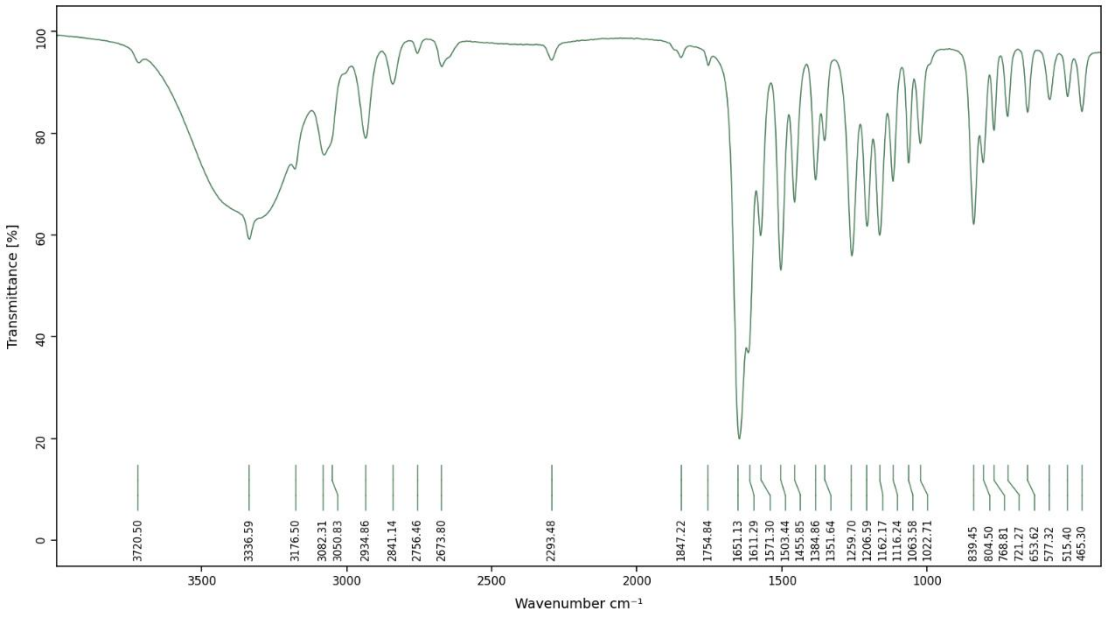

Figure 3.6: FTIR Spectra of Oroxylin A

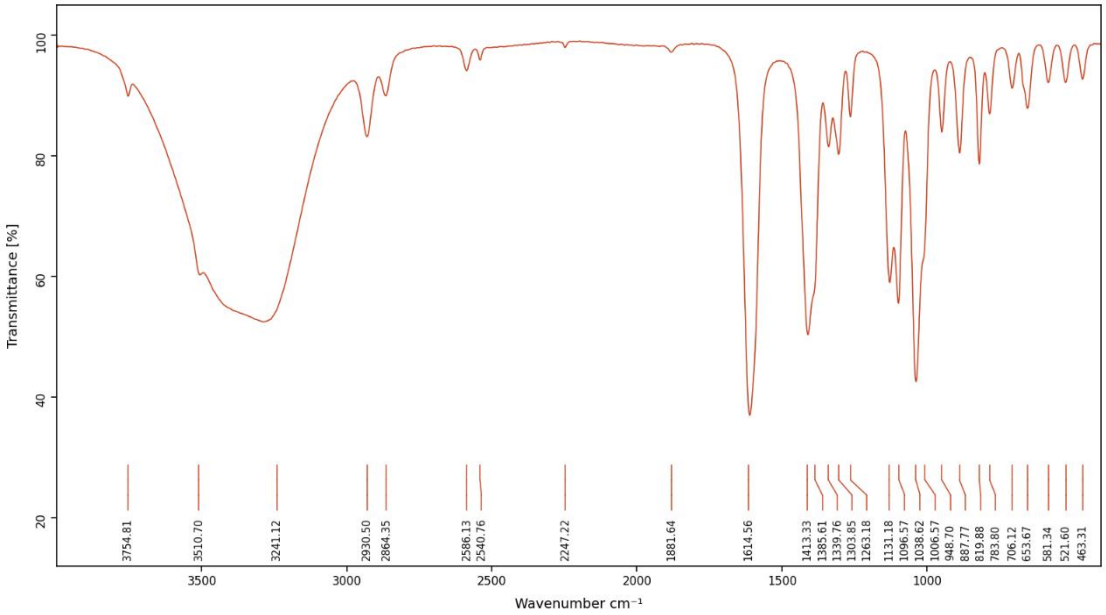

Figure 3.7: FTIR Spectra of Sodium Alginate

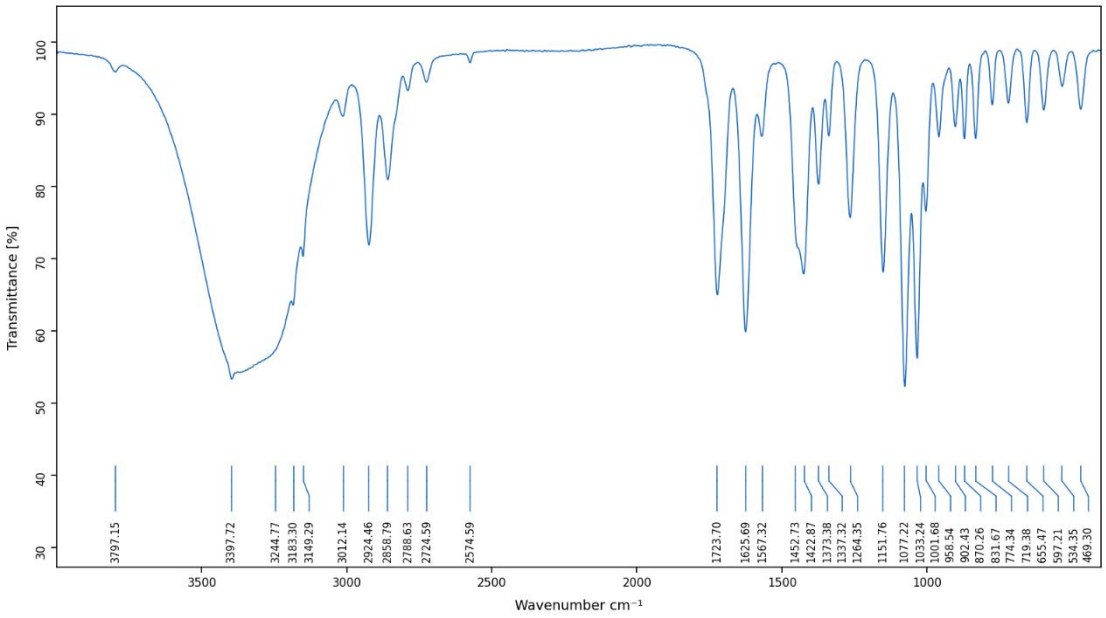

Figure 3.8: FTIR Spectra of *Boswellia serrata* gum

Table 3.9: FTIR Spectral Analysis of Oroxylin A, Sodium Alginate, Boswellia Serrata Gum, and Physical Mixture

Functional Group	Standard Wavenumber (cm^{-1})	Oroxylin A (Pure Drug)	Sodium Alginate	Boswellia Serrata Gum	Physical Mixture
O–H Stretching	3200–3600	3336.59	3241.12	3397.72	3142.40
C–H Aromatic Stretching	3000–3100	3082.31, 3050.83	—	3012.14	3093.62, 3037.43
C–H Aliphatic Stretching	2850–2950	2934.86, 2841.14	2930.50	2924.46	2927.81, 2854.51
C=O Stretching (Carbonyl)	1650–1750	1651.13	—	1723.70	1724.16
C=C Aromatic Stretching	1580–1650	1611.30, 1571.20	1614.56	1625.69	1638.35, 1611.43
C=C Ring Stretching	1400–1500	1503.44, 1455.85	1413.33	1452.73	1459.25
O–H Bending	1350–1390	1384.86, 1351.64	1385.61	1375.38	1382.57, 1350.77
C–O–C Stretching (Ether/OCH_3)	1200–1270	1259.70, 1206.59	—	—	1261.52
C–O Stretching	1000–1100	1162.17, 1126.17, 1085.58, 1022.71	1038.62, 1096.57	1033.24, 1077.22	1043.56, 1097.70
C–H Bending (Aromatic)	650–900	839.45, 804.50	887.88	870.26	894.12
C=O Bending	400–700	653.62, 577.32, 515.40, 465.30	581.34, 521.60, 463.31	655.47, 534.35, 469.30	650.48, 585.82, 525.47, 457.28

3.1.6. Optimization of Oroxylin A loaded Inhalable Microspheres

A. ANOVA for Quadratic Model for Particle Size

The quadratic model was found to be the best fit for particle size with an adjusted R^2 of 0.9904 and predicted R^2 of 0.9573, demonstrating excellent predictability. The ANOVA results confirmed the model was statistically significant (F-value = 166.19, p = 0.0007). Among the independent variables, sodium alginate (B) exhibited the most significant influence on particle size (p = 0.0002, F = 567.34), followed by *Boswellia serrata* gum (A) (p = 0.0006). The interaction term AB (p = 0.1918) and quadratic term A^2 (p = 0.3123) were non-significant, while B^2 was significant (p = 0.0132). The contour and 3D response surface plots further illustrated the positive effect of both polymers on particle size.

Table 3.10: Model fit summary for particle size

Source	Sequential p-value	Lack of Fit p-value	Adjusted R^2	Predicted R^2	
Linear	< 0.0001		0.9436	0.9083	
2FI	0.5392		0.9377	0.8348	
Quadratic	**0.0281**		**0.9904**	**0.9573**	**Suggested**
Cubic	0.2625		0.9980	0.9548	**Aliased**

Regression equation obtained for particle size is as follows:

Particle Size = 3.69111 + 0.591667 * A + 0.926667 * B + 0.08 * AB + -0.0816667 * A^2 + -0.356667 * B^2

Table 3.11: ANOVA for quadratic model for Particle Size

Source	Sum of Squares	df	Mean Square	F-value	p-value	
Model	7.55	5	1.51	166.19	0.0007	significant
A-Boswellia serrata Gum	2.10	1	2.10	231.29	0.0006	
B-Sodium Alginate	5.15	1	5.15	567.34	0.0002	
AB	0.0256	1	0.0256	2.82	0.1918	
A^2	0.0133	1	0.0133	1.47	0.3123	
B^2	0.2544	1	0.2544	28.02	0.0132	
Residual	0.0272	3	0.0091			
Cor Total	7.57	8				

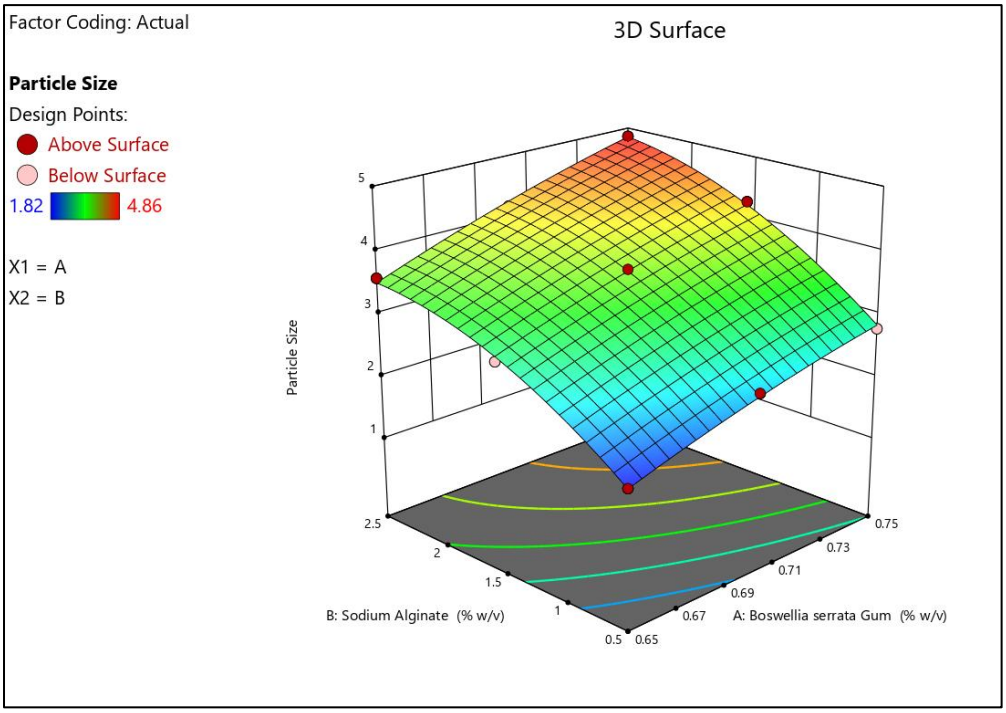

Figure 3.12: 3D plot showing effect of sodium alginate and *Boswellia serrata* on particle size

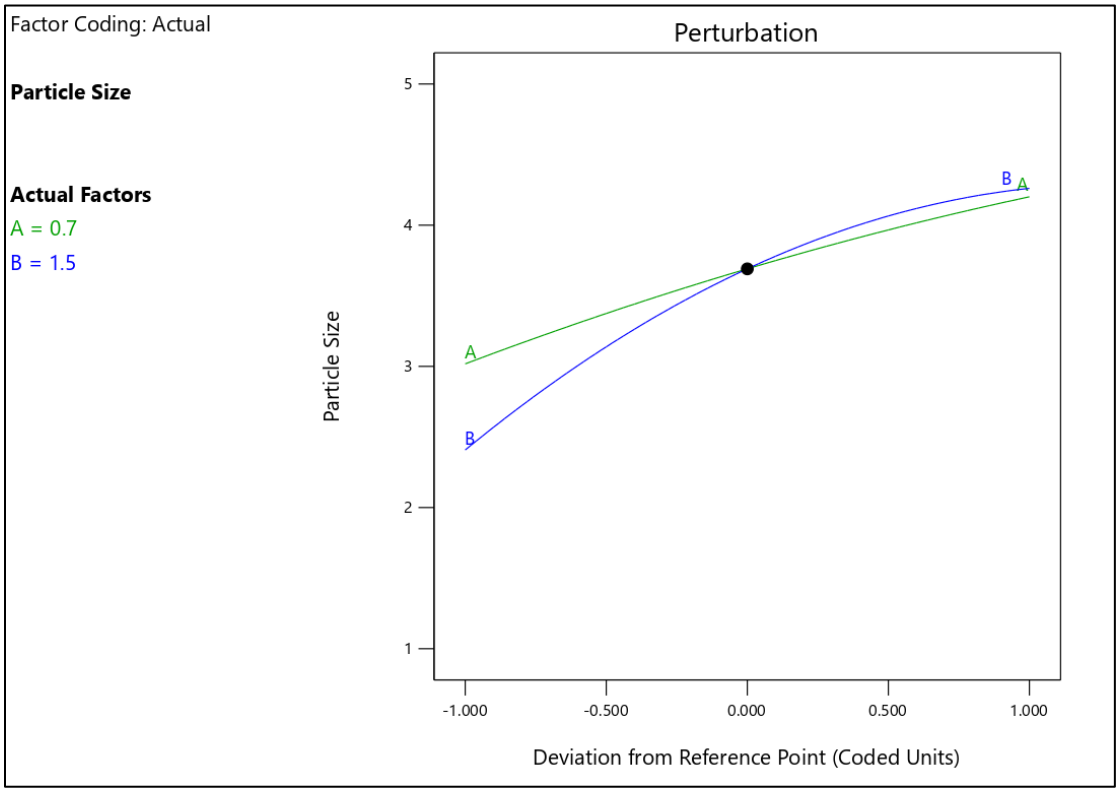

Figure 3.13: Perturbation plot showing influence of concentrations of each independent variables on particle size

3.1.7. Stability study

The optimized formulation (F1) was evaluated for stability under accelerated and room temperature conditions for 3 months as per ICH guidelines.Under accelerated conditions, slight changes were observed, including minor color change, slight increase in particle size, and small reductions in entrapment efficiency and drug release, indicating minimal degradation.At room temperature, no significant changes were noted in all parameters ($p > 0.05$), confirming good stability.

4.0. DISCUSSION:

The study aimed to develop and optimize oroxylin A-loaded inhalable microspheres using sodium alginate and Boswellia serrata gum via ionotropic gelation for pulmonary drug delivery. Oroxylin A, a bioactive flavonoid, has significant pharmacological activities but suffers from poor solubility and low oral bioavailability, making pulmonary delivery a suitable alternative.

Preformulation studies confirmed drug identity and purity (λmax 273 nm, R^2 = 0.9997) and classified it as BCS Class II. Compatibility studies (DSC, FTIR) showed no interaction between drug and polymers.

Microspheres (F1–F9) were successfully prepared with particle sizes (1.82–4.86 µm) suitable for lung deposition. Increased polymer concentration led to larger particle size, higher entrapment efficiency, and slower drug release. All formulations showed good flow properties and stability.

In vitro release exhibited a biphasic pattern with sustained release up to 12 hours, best fitting the Higuchi diffusion model. Optimized formulation

(F1) showed highest drug release (~92%) and good stability

5.0 CONCLUSION:

The procured oroxylin A sample was confirmed for its identity, purity, and physicochemical characteristics through organoleptic evaluation, UV-Visible spectroscopy (λmax 273 nm), melting point determination (232.33 ± 0.58°C), and spectral analyses. The solubility study established oroxylin A as a BCS Class II compound with poor aqueous solubility, thereby justifying the need for an alternative drug delivery approach. The DSC and FTIR compatibility studies confirmed the absence of any physical or chemical incompatibility between oroxylin A and the selected polymeric excipients, sodium alginate and Boswellia serrata gum, supporting their combined use in the microsphere formulation. The ionotropic gelation technique proved to be a simple, reproducible, and efficient method for the preparation of oroxylin A loaded inhalable microspheres. The 3^2 full factorial design successfully optimized the formulation parameters, and the quadratic model demonstrated excellent predictive capability with high statistical significance for both particle size and in vitro drug release responses. Among the independent variables, sodium alginate exhibited a more dominant influence on both responses compared to Boswellia serrata gum.

The optimized formulation F1, containing the lowest concentrations of sodium alginate (0.50% w/v) and Boswellia serrata gum (0.65% w/v), was identified as the most desirable formulation exhibiting the smallest particle size (1.82 ± 0.14 µm) within the respirable range, highest cumulative drug release (92.14 ± 2.48%) at 12 hours, adequate zeta potential (-18.42 ± 1.12 mV), satisfactory drug entrapment efficiency (62.18 ± 1.54%), and good flow properties. The drug release from the microspheres followed a diffusion-controlled mechanism as confirmed by the Higuchi kinetic model ($R^2 = 0.9946$). The SEM analysis confirmed the spherical morphology and smooth surface texture of the prepared microspheres. The stability study conducted as per ICH Q1A (R2) guidelines demonstrated that the optimized formulation F1 exhibited satisfactory stability at room temperature (25 ± 2°C / 60 ± 5% RH) over a period of 3 months with no statistically significant changes in the evaluated parameters, confirming its suitability for storage under ambient conditions.

REFERENCES

1. Loeb LA, Emster VL, Warner KE, Abbotts J, Laszlo J. Smoking and Lung Cancer: An Overview1,2. Cancer Res 1984;44:5940–58.
2. Ambrosini V, Nicolini S, Caroli P, Nanni C, Massaro A, Marzola MC, et al. PET/CT imaging in different types of lung cancer: An overview. Eur J Radiol 2012;81:988–1001. https://doi.org/10.1016/j.ejrad.2011.03.020.
3. Petrella F, Rizzo S, Attili I, Passaro A, Zilli T, Martucci F, et al. Stage III Non-Small-Cell Lung Cancer: An Overview of Treatment Options. Curr Oncol 2023;30:3160–75. https://doi.org/10.3390/curroncol30030239.
4. Eltayeb K, La Monica S, Tiseo M, Alfieri R, Fumarola C. Reprogramming of Lipid Metabolism in Lung Cancer: An Overview with Focus on EGFR-Mutated Non-Small Cell Lung Cancer. Cells 2022;11:413. https://doi.org/10.3390/cells11030413.
5. Peng L, Shang Q-W, Deng H-Y, Liu Z-K, Li W, Wang Y. Lobe-specific lymph node dissection in early-stage non-small-cell lung cancer: An overview. Asian J Surg 2023;46:683–7. https://doi.org/10.1016/j.asjsur.2022.07.042.

6. Yang T, Wu C, Li P, Zhong Y, Wu W, Wang S, et al. Efficacy and Safety of Huachansu as an Adjuvant Therapy for Non-Small Cell Lung Cancer: An Overview of Systematic Reviews and Meta-Analyses. Integr Cancer Ther 2024;23:15347354241237234.https://doi.org/10.1177/15347354241237234.
7. Ruano-Ravina A, Martin-Gisbert L, Kelsey K, Pérez-Ríos M, Candal-Pedreira C, Rey-Brandariz J, et al. An overview on the relationship between residential radon and lung cancer: what we know and future research. Clin Transl Oncol 2023;25:3357–68. https://doi.org/10.1007/s12094-023-03308-0.
8. Ruano-Ravina A, Martin-Gisbert L, Kelsey K, Pérez-Ríos M, Candal-Pedreira C, Rey-Brandariz J, et al. An overview on the relationship between residential radon and lung cancer: what we know and future research. Clin Transl Oncol 2023;25:3357–68. https://doi.org/10.1007/s12094-023-03308-0.
9. Dunn B, Pierobon M, Wei Q. Automated Classification of Lung Cancer Subtypes Using Deep Learning and CT-Scan Based Radiomic Analysis. Bioengineering 2023;10:690. https://doi.org/10.3390/bioengineering10060690.
10. Halder A, Dey D. MorphAttnNet: An Attention-based morphology framework for lung cancer subtype classification. Biomed Signal Process Control 2023;86:105149. https://doi.org/10.1016/j.bspc.2023.105149.
11. Barbouchi K, El Hamdi D, Elouedi I, Aïcha TB, Echi AK, Slim I. A transformer-based deep neural network for detection and classification of lung cancer via PET/CT images. Int J Imaging Syst Technol 2023;33:1383–95. https://doi.org/10.1002/ima.22858.
12. Zhao H, Su Y, Wang M, Lyu Z, Xu P, Jiao Y, et al. The Machine Learning Model for Distinguishing Pathological Subtypes of Non-Small Cell Lung Cancer. Front Oncol 2022;12:875761. https://doi.org/10.3389/fonc.2022.875761.
13. Lin J, Yu Y, Zhang X, Wang Z, Li S. Classification of Histological Types and Stages in Non-small Cell Lung Cancer Using Radiomic Features Based on CT Images. J Digit Imaging 2023;36:1029–37. https://doi.org/10.1007/s10278-023-00792-2.
14. Vicidomini G. Current Challenges and Future Advances in Lung Cancer: Genetics, Instrumental Diagnosis and Treatment. Cancers 2023;15:3710. https://doi.org/10.3390/cancers15143710.
15. Siddheshwar SS, Jagtap D, Mankar SD, Ghorpade AC, Dighe SB, Bhawar S. Development and Optimization of Myricetin Loaded Inhalable Microsphere to Treat COPD. Pharm Res 2025;42:2063–78. https://doi.org/10.1007/s11095-025-03973-6.
16. Sharma Y, Mahar R, Chakraborty A, Nainwal N. Optimizing the formulation variables for encapsulation of linezolid into polycaprolactone inhalable microspheres using double emulsion solvent evaporation. Tuberculosis 2023;143:102417. https://doi.org/10.1016/j.tube.2023.102417.
17. Mahar R, Chakraborty A, Nainwal N. Formulation of Resveratrol-Loaded Polycaprolactone Inhalable Microspheres Using Tween 80 as an Emulsifier: Factorial Design and Optimization. AAPS PharmSciTech 2023;24:131. https://doi.org/10.1208/s12249-023-02587-8.
18. Hiremath JN, Iliger SR, Badalamoole V, Manjunath HR, Raghu AV. Gellan Gum-Sodium Alginate Novel pH-Sensitive Microspheres: Formulation and Characterization for Chronotherapy of Arthritis. ChemistrySelect 2024;9:e202401055. https://doi.org/10.1002/slct.202401055.

19. Harwansh RK, Deshmukh R. Formulation and Evaluation of Sodium Alginate and Guar Gum Based Glycyrrhizin Loaded Mucoadhesive Microspheres for Management of Peptic Ulcer. Indian J Pharm Educ Res 2021;55:728–37. https://doi.org/10.5530/ijper.55.3.145.
20. Behrend-Keim B, Castro-Muñoz A, Monrreal-Ortega L, Ávalos-León B, Campos-Estrada C, Smyth HDC, et al. The forgotten material: Highly dispersible and swellable gelatin-based microspheres for pulmonary drug delivery of cromolyn sodium and ipratropium bromide. Int J Pharm 2023;644:123331. https://doi.org/10.1016/j.ijpharm.2023.123331.
21. Quality by Design Approach for Formulation and Optimization of Microparticles Based Inhalable Phytopharmaceuticals of Trigonella Foenum-Graecum and Alpinia Galanga. Biointerface Res Appl Chem 2021;12:2050–67. https://doi.org/10.33263/BRIAC122.20502067.
22. Almansour K, Alfagih IM, Aodah AH, Alheibshy F, Ali R, Al Hagbani T, et al. Inhalable, Spray-Dried Terbinafine Microparticles for Management of Pulmonary Fungal Infections: Optimization of the Excipient Composition and Selection of an Inhalation Device. Pharmaceutics 2022;14:87. https://doi.org/10.3390/pharmaceutics14010087.
23. Amran M, Khafagy E-S, Mokhtar HI, Zaitone SA, Moustafa YM, Gad S. Formulation and Evaluation of Novel Additive-Free Spray-Dried Triamcinolone Acetonide Microspheres for Pulmonary Delivery: A Pharmacokinetic Study. Pharmaceutics 2022;14:2354. https://doi.org/10.3390/pharmaceutics141123.

HOW TO CITE: Mayur Avinash Lawande*, Wagh.j.G, Development and Characterization of oroxylin A loaded Functionalized inhalable microspheres for targeted delivery in lung cancer, Int. J. of Pharm. Sci., 2026, Vol 4, Issue 5, 7451-7468. https://doi.org/10.5281/zenodo.20416115